Lasers in Surgery and Medicine 39:145–155 (2007)

The Effects of Pulse Energy Variations on the Dimensions of Microscopic Thermal Treatment Zones in Nonablative Fractional Resurfacing

Vikramaditya P. Bedi, MS,[1] Kin Foong Chan, PhD,[1]* R. Kehl Sink, PhD,[1] Basil M. Hantash, MD, PhD,[1,2] G. Scott Herron, MD, PhD,[3] Zakia Rahman, MD,[1,2] Steven K. Struck, MD,[4] and Christopher B. Zachary, MBBS, FRCP[5]

[1]*Reliant Technologies, Inc., Mountain View, California 94043*
[2]*Stanford University School of Medicine, Stanford, California 94305*
[3]*Palo Alto Medical Foundation, Palo Alto, California 94301*
[4]*Struck Plastic Surgery, Atherton, California 94027*
[5]*University of California, Irvine, California 92697*

Background and Objectives: We examined the effects of pulse energy variations on the dimensions of microscopic thermal injury zones (MTZs) created on human skin ex vivo and in vivo using nonablative fractional resurfacing.

Materials and Methods: A Fraxel® SR laser system emitting at 1,550 nm provided an array of microscopic spots at variable densities. Pulse energies ranging from 4.5 to 40 mJ were tested on human abdominal skin ex vivo and in vivo. Tissue sections were stained with hematoxylin and eosin (H&E) or nitro blue tetrazolium chloride (NBTC) and MTZ dimensions were determined. Ex vivo and in vivo results were compared. Dosimetry analyses were made for the surface treatment coverage calculation as a function of pulse energy and collagen coagulation based on H&E stain or cell necrotic zone based on NBTC stain.

Results: Each MTZ was identified by histological detection of a distinct region of loss of tissue birefringence and hyalinization, representing collagen denaturation and cell necrosis within the irradiated field immediately, 1, 3, and 7 days after treatment. At high pulse energies, the MTZ depth could exceed 1 mm and width approached 200 μm as assessed by H&E. NBTC staining revealed viable interlesional tissue. In general, no statistically significant difference was found between in vivo and ex vivo depth and width measurements.

Conclusions: The Fraxel® SR laser system delivers pulses across a wide range of density and energy levels. We determined that increases in pulse energy led to increases in MTZ depth and width without compromising the structure or viability of interlesional tissue. Lasers Surg. Med. 39:145–155, 2007. © 2006 Wiley-Liss, Inc.

Key words: dermatology; remodeling; rejuvenation; wrinkles; resurfacing; photoaging; Fraxel; MTZ; denaturation; collagen; infrared laser

INTRODUCTION

The Fraxel® SR laser system is a device that emits a quasi-collimated beam at 1,550 nm. The treatment provided by this device follows the principle of fractional photothermolysis [1] and resurfacing. The laser system scans an array of spatially separated microbeams across the surface of the skin to create a pattern of thermal injuries, known as microscopic treatment zones (MTZs), within the field of irradiation while sparing interlesional tissue. The degree of epidermal and dermal tissue coagulation depends on factors such as pulse energy and density. The pulse energy can be adjusted to obtain a variety of MTZ depths and widths. Through the use of a motion-sensing feedback loop, the density of MTZs is kept constant as the handpiece speed is varied by the user. The scanning handpiece randomly lays down an array of MTZs over consecutive passes thus preventing gaps in treatment and providing a more natural appearance. This continuous track-and-scan technique reduces the appearance of Moiré patterns, a phenomenon that results from overlapping or multi-pass treatments using a regular grid array or stamp pattern.

As a result of rapid epidermal turnover, necrotic debris can be found at the level of the stratum corneum, overlying each MTZ 24 hours after treatment [1]. This material has been termed microscopic epidermal necrotic debris (MEND). It is hypothesized that rapid epidermal turnover with subsequent exfoliation of the MEND acts in concert with reepithelialization of the irradiated epidermal field. This explains in part the ability of fractional photothermolysis [1] to promote skin rejuvenation through non-ablative laser resurfacing. Additional benefits arise from the long-term wound healing response, which leads to replacement of photoaged dermal tissue with newly deposited collagen. Thus, in contrast to ablative skin resurfacing with devices such as the pulsed CO_2 or Er:YAG

*Correspondence to: Kin F. Chan, PhD, Reliant Technologies, Inc. 464 Ellis Street, Mountain View, CA 94043.
E-mail: kchan@reliant-tech.com
Accepted 4 August 2006
Published online 9 November 2006 in Wiley InterScience (www.interscience.wiley.com).
DOI 10.1002/lsm.20406

lasers [2–10], nonablative fractional resurfacing by a pulsed mid-infrared laser is able to achieve photorejuvinative effects in the absence of significant side effects and downtime [1].

Ablative resurfacing devices such as the pulsed Er:YAG or CO_2 are also limited by their inability to remove more than 5–30 μm of tissue with each pass in the absence of pulse stacking [11], making these devices impractical for the coagulation of deeper tissue with thermal damage zones limited to less than 150 μm. A dual-mode Er:YAG laser has been shown to only achieve ablation depths up to 200 μm, again with a limited thermal damage zone up to 150 μm. Mid-infrared nonablative fractional resurfacing may have the potential to produce deeper microscopic tissue coagulation or thermal damage with significant clinical benefits while sparing adjacent tissue to reduce downtime.

For the purpose of this report, we have defined the dimension of each MTZ (or lesion) as the zone of collagen denaturation as measured histologically by hematoxylin & eosin (H&E) staining [12] or the zone of non-viable cells as measured histologically by nitro blue tetrazolium chloride (NBTC) [13–14]. Previous work has shown the former method to be essentially equivalent to measurement of the loss of birefringence by cross-polarization microscopy of laser-induced thermal coagulation [15].

In this study, we analyzed the effect of pulse energy on the dimensions of the MTZs, both in vivo and ex vivo using histochemical techniques and light microscopy. An ex vivo model was designed to correlate with the in vivo conditions. Our results suggest no significant statistical difference between lesion dimensions measured in vivo and ex vivo.

METHODS

Ex Vivo Study

Ex vivo tests were performed using freshly excised human abdominal skin samples (Fitzpatrick skin types II–IV) in order to determine the physical dimensions of individual MTZs after treatment with the 1550-nm Fraxel® SR laser system (Reliant Technologies, Inc.,

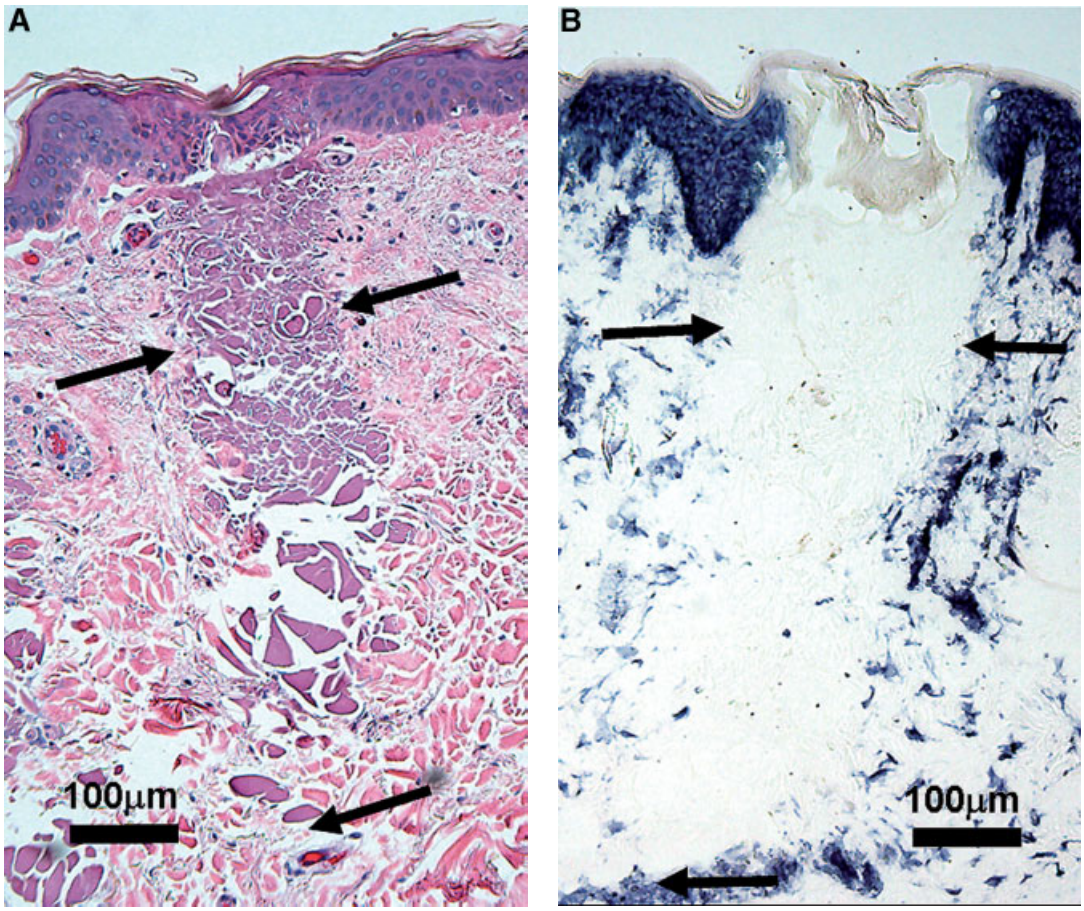

Fig. 1. In vivo human abdominal tissue treated with the Fraxel® SR laser at 20 mJ (final spot density of 500 MTZ/cm^2, optical magnification 10×). The sample was excised immediately post-treatment. **A**: A paraffin embedded H&E stained section shows a quasi-cylindrical thermal treatment zone corresponding to an individual thermal wound, and (**B**) a frozen NBTC stained section of treated skin shows loss of dermal and epidermal cell viability within the irradiated zone.

Mountain View, CA) at varying pulse energies between 6 and 40 mJ.

In the standard clinical operating mode, the laser handpiece tracks the relative velocity of the handpiece with respect to the skin and adjusts the firing rate of the laser to create the desired density of MTZs. For the ex vivo tests, the velocity tracking system was disabled and the handpiece was translated at a specified speed using a precision linear stage driven by an ESP 300 motion controller (Newport Co., Irvine, CA).

The subcutaneous fat was trimmed from each skin sample. Each skin sample was cut to a size of 10 mm×60 mm and hairs within the test sites were shaved. The sample was sandwiched between two saline soaked 4″×4″ gauze pads. The sandwich was then heated on a digital hot plate (Cole-Parmer Instrument Co., Vernon Hills, IL) until the surface of the skin reached a temperature of 98°F as measured with a Minitemp® MT4 infrared probe (Raytek Corporation, Santa Cruz, CA). Immediately prior to treatment, the top layer of gauze was removed. The lower gauze and tissue sample were then placed on an aluminum hot plate set at 98°F. The exposed skin temperature was measured to be 98 ± 3°F prior to treatment. The laser handpiece was not heated prior to treatment. Each laser treatment covered the entire length of the skin sample. Pulse energy for the treatments ranged from 4.5 to 40 mJ. Since the system was operated in the manual mode, the actual pulse energy at each setting was measured and recorded. One to six passes at a velocity of 0.4–3.4 cm/seconds were made in one direction to create final spot densities of 250–1,500 MTZ/cm^2. Samples were then embedded in optimal cutting temperature compound (IMEB, Inc., San Marcos, CA) or fixed in 10% v/v neutral buffered formalin (VWR International, West Chester, PA) for frozen or paraffin sectioning, respectively. The samples were sliced into 10–20 μm thick sections and stained with H&E.

In Vivo Study

Five healthy subjects received abdominal treatments with the Fraxel® SR laser system prior to undergoing abdominoplasty. The study protocol was approved by an institutional review board, and each subject was consented before participating in the study. Hairs within the test sites

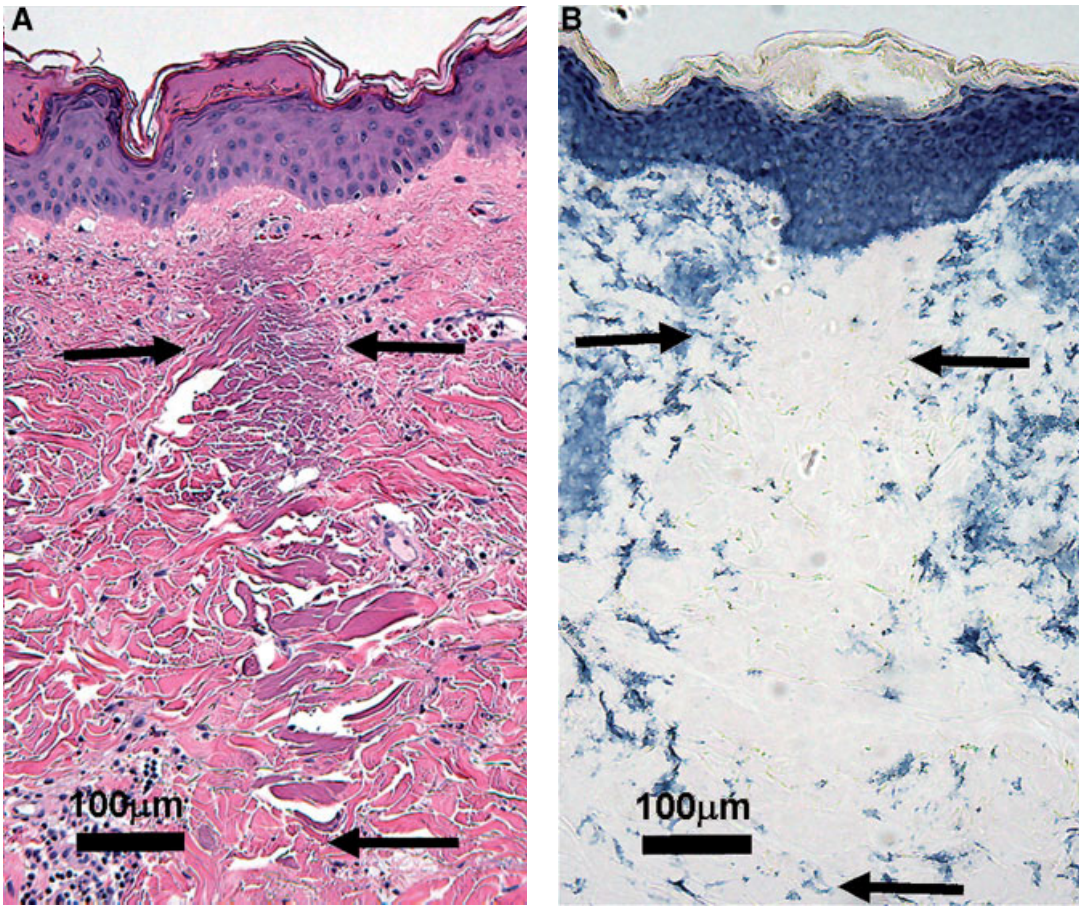

Fig. 2. In vivo human abdominal tissue treated at 20 mJ and excised 3 days post-treatment (final spot density of 500 MTZ/cm^2, optical magnification 10×). **A**: A paraffin embedded H&E stained section, and (**B**) a frozen NBTC stained section of treated skin shows a MEND overlying the thermal treatment zone. The epidermis and DE junction are healed.

were shaved prior to laser treatment. Subjects were pretreated with either general anesthesia plus topical petrolatum or topical lidocaine, depending on whether their laser treatment was immediately or 1–7 days prior to abdominoplasty, respectively. The handpiece was operated in the standard clinical operating mode allowing for the creation of a constant density of MTZs. Each laser treatment covered approximately 12 cm^2, with pulse energy settings at 6, 10, 12, 15, 20, 30, 35, and 40 mJ, for a total of eight sites on the abdomen. Since the system was operating in the standard clinical operating mode, it was not possible to measure the actual pulse energy delivered at each setting before treatment; the actual pulse energy was assumed to be within $\pm 20\%$ of its corresponding set value based on manufacturer calibration and specification. The treated abdominal skin was excised during the abdominoplasty, which occurred immediately, 1, 3, or 7 days following laser treatment. Specimens were extracted throughout the 12-cm^2 area of each treatment site, and thereafter, the skin samples were prepared identically to those of ex vivo tests.

Statistical Analyses

For each data point, at least 10 lesion samples were evaluated ($n \geq 10$). At parameters where many lesions were properly sectioned and found to be appropriate for evaluation (see two paragraphs below), as many as 30 lesion samples were evaluated. Since small variations in the angle of sectioning with the cryotome or microtome could mean significant differences in the apparent depth of the MTZs, a test run of successive histology sections were performed at a few pulse energy levels. By following them out section by section, we obtained a good idea of the maximum width and depth of lesions attainable at each parameter. We used this experience as a guideline to select lesions that were representative of each pulse energy parameter for the specimen.

Images of H&E and NBTC stained histology slides were recorded using a DM LM/P microscope and a DFC320 digital camera (Leica Microsystem, Cambridge, UK). Histology images were evaluated by identifying the well-demarcated boundaries of the thermal lesions on the H&E and NBTC stained histology images. Measurements

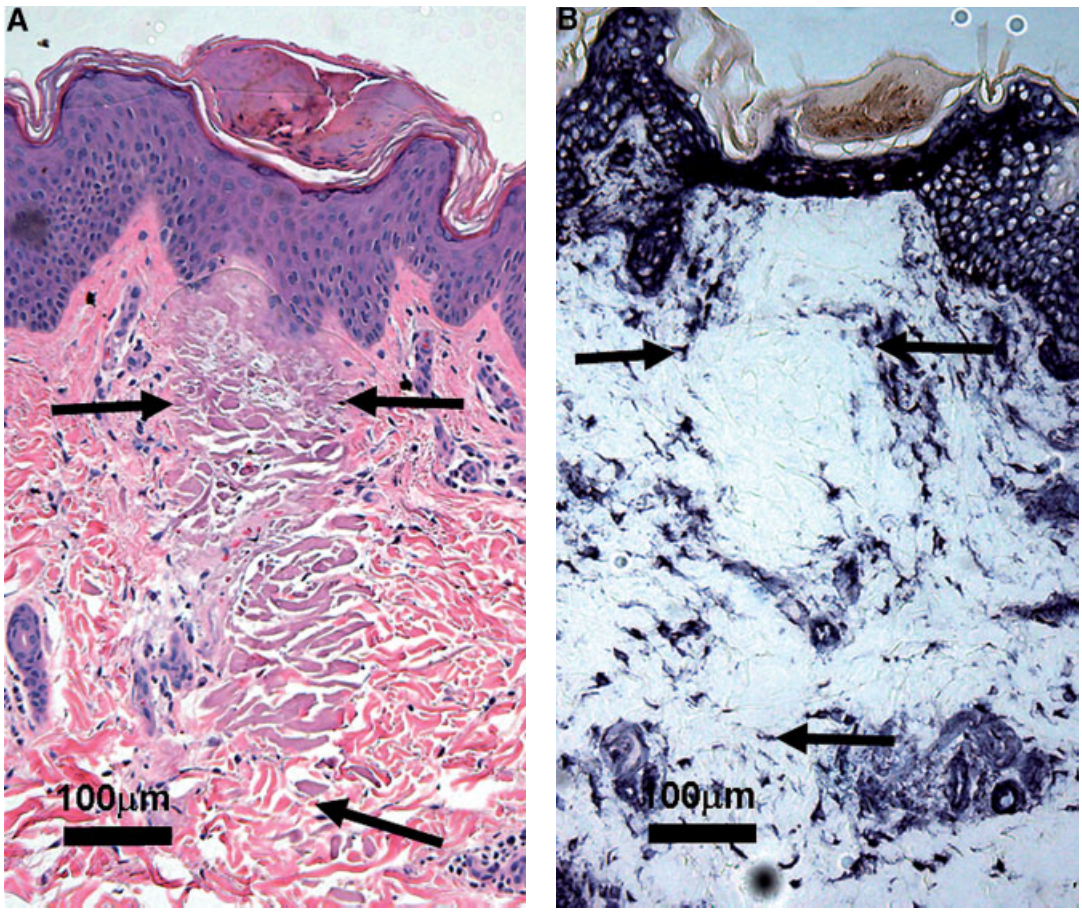

Fig. 3. In vivo human abdominal tissue treated at 20 mJ and excised 7 days post-treatment (final spot density of 1,000 MTZ/cm^2, optical magnification 10×). **A**: A paraffin embedded H&E stained section, and (**B**) a frozen NBTC stained section of treated skin shows an exfoliating MEND at the surface of the epidermis. Note migration of inflammatory cells into the dermal coagulation zone, and exfoliation of MEND formation containing necrotic debris.

of lesion dimensions were made with a proprietary Visual Basic® computer program (Reliant Technologies, Inc.).

Lesions were selected for measurements based on a few guidelines. As mentioned before, since the Fraxel® SR laser system creates quasi-cylindrical microscopic lesions with a large aspect ratio (i.e., high lesion depth-to-width ratio), it was relatively difficult to ensure during histological processing that lesions were sectioned across the ideal plane. Therefore, only those images which captured an entire lesion width and depth were evaluated (~20% of the total). The following sections were excluded: (i) lesions that did not have a superficial component within the epidermis, (ii) lesions that were adjacent to one or more other lesions that did not have a superficial component within the

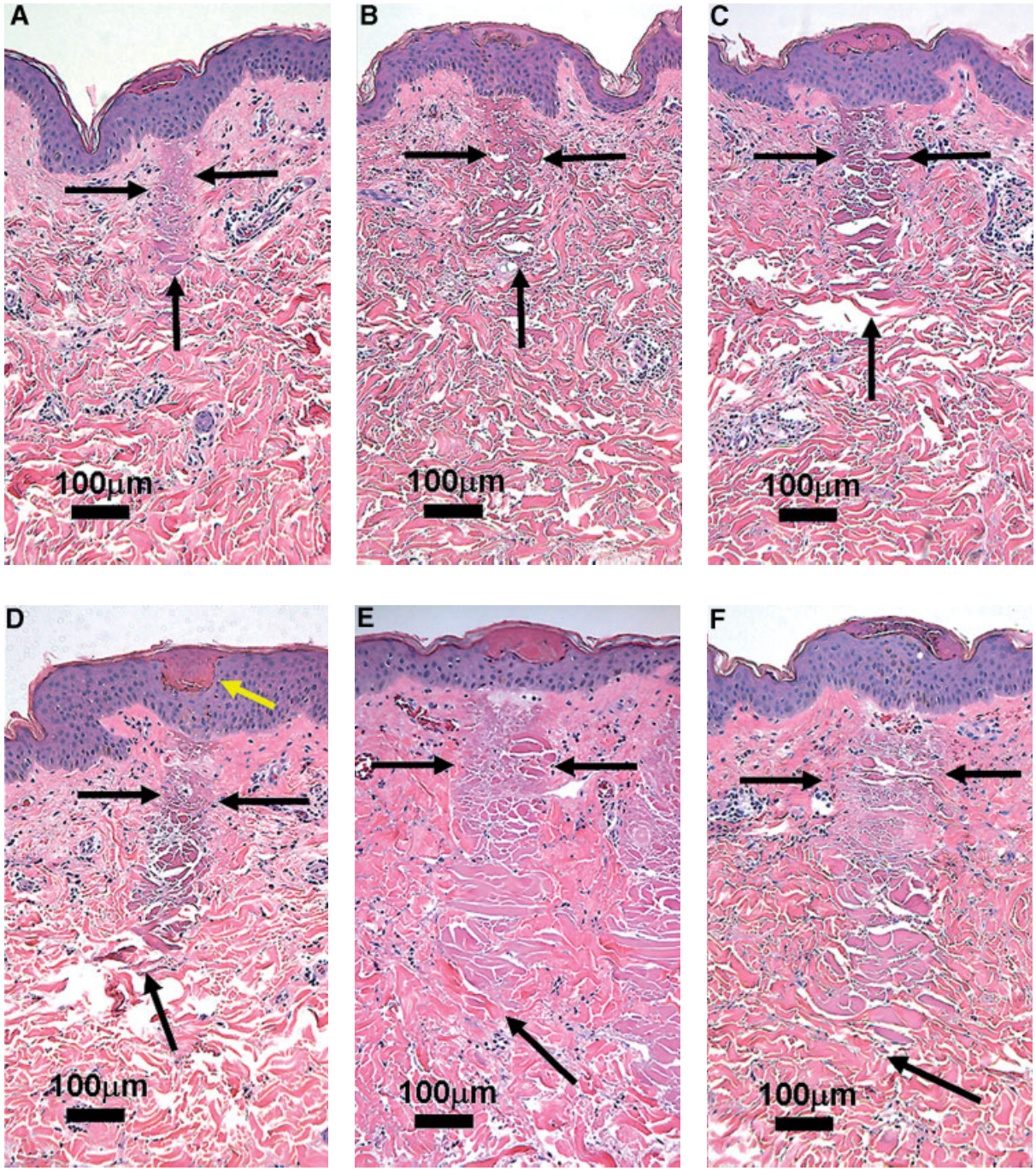

Fig. 4. Composite histology images from the in vivo study (optical magnification 10×). The paraffin embedded H&E stained sections show MTZs 1 day post-treatment for pulse energies of (**A**) 6, (**B**) 10, (**C**) 12, (**D**) 15, (**E**) 20, (**F**) 25, (**G**) 30, and (**H**) 35 mJ.

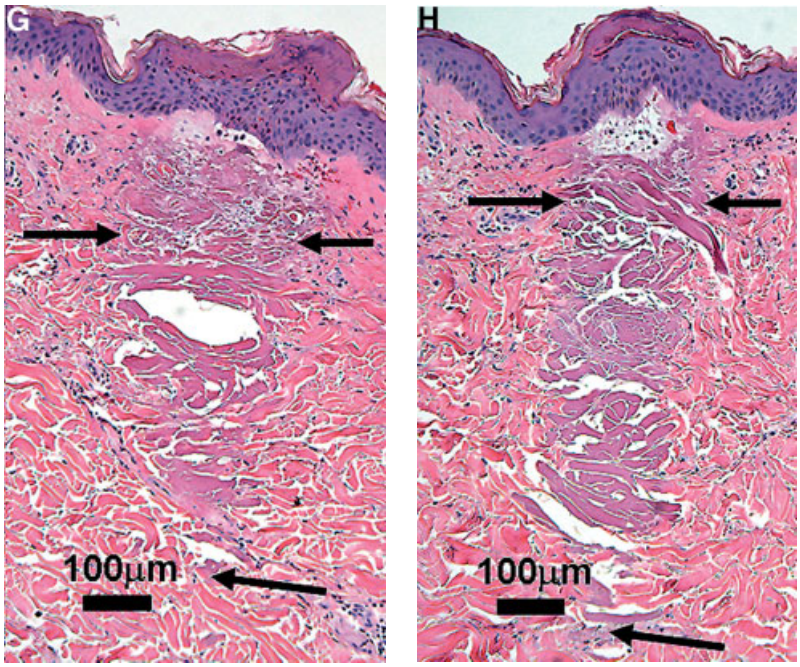

Fig. 4. (*Continued*)

epidermis, (iii) lesions with a superficial component that appeared to be more than 20% shallower than the deepest known lesions for that particular sample, (iv) lesions that appeared to be more than 20% narrower than the widest known lesions for that particular sample, and (v) lesions that had an uncharacteristic shape.

The ex vivo model was performed first in this series of experiment, and its results compared to the in vivo model.

RESULTS

In the in vivo study, laser exposures produced a pattern of MTZs that were separated by viable tissue. Sections stained with H&E and NBTC were imaged to evaluate the MTZs immediately, 1, 3, or 7 days post-treatment. Figures 1–3 show images of H&E and NBTC stained sections excised from subjects treated with a pulse energy of 20 mJ. Each of these figures shows clearly demarcated, quasi-cylindrical MTZs that extended into the dermis. With the exception of reepithelialization of the epidermis in Figures 2B and 3B, the NBTC stained images shown in Figures 1B, 2B, and 3B confirm the total loss of epidermal and dermal cell viability within the confines of the MTZ. Cross polarization microscopy further demonstrated that collagen was denatured within each MTZ (data not shown). No significant difference in the dimensions of the denaturation zone was detected by cross polarization versus H&E.

We examined the wound healing process for each MTZ at various times post-treatment. Immediately after treatment at 20 mJ, MTZs of approximately 700 μm in depth and 150 μm in width were observed by H&E staining. Within 1 day post-treatment (Fig. 4D), a collection of necrotic debris approximately 60×150 μm on average (yellow arrow) in cross section was observed to overlie each thermal treatment zone, consistent with our previous study [1]. Within 1–3 days post-treatment, the dermal-epidermal junction (DE) junction appeared partially repaired (Figs. 4D and 2A) and epidermal cellular viability assessed by NBTC staining was restored (Fig. 2B). The stratum corneum overlying the MTZ remained intact. At day 7, the epidermis and DE junction returned to normal structure and exfoliation of the compacted MEND was observed (Fig. 3). Staining with NBTC revealed migration of inflammatory cells within the coagulation zone (Fig. 3B). No significant difference in size of the coagulation zone was detected by H&E staining for sections obtained 0, 1, 3, and 7 days post-treatment at each energy parameter.

Figure 4 shows a composite of paraffin embedded H&E histology images at 1 day post-treatment at 6–35 mJ. Separation of the DE junction was most prevalent at pulse energies exceeding 20 mJ (Fig. 4F–H). Despite disruption of the DE junction, the stratum corneum remained intact at all pulse energies tested and showed no histologic abnormalities by either staining method. The measured widths and depths of the thermal treatment zones, demarcated by H&E staining, increased quasi-linearly with pulse energy from 6 to 40 mJ (Fig. 5). At 40 mJ, the measured depths exceeded 1 mm (mean depth ~950 μm) and the widths approached 200 μm (Fig. 5B, H&E stain). The depth-to-width ratios of the in vivo lesions at all energy parameters remained relatively constant with a mean of 5.1 ± 0.3 based on H&E stain histology.

Ex vivo histology results were analyzed against the in vivo results. In general, no statistically significant difference was observed between lesion dimensions obtained in vivo and ex vivo ($P > 0.05$) with the exception of three out of sixteen data points (i.e., eight data points for

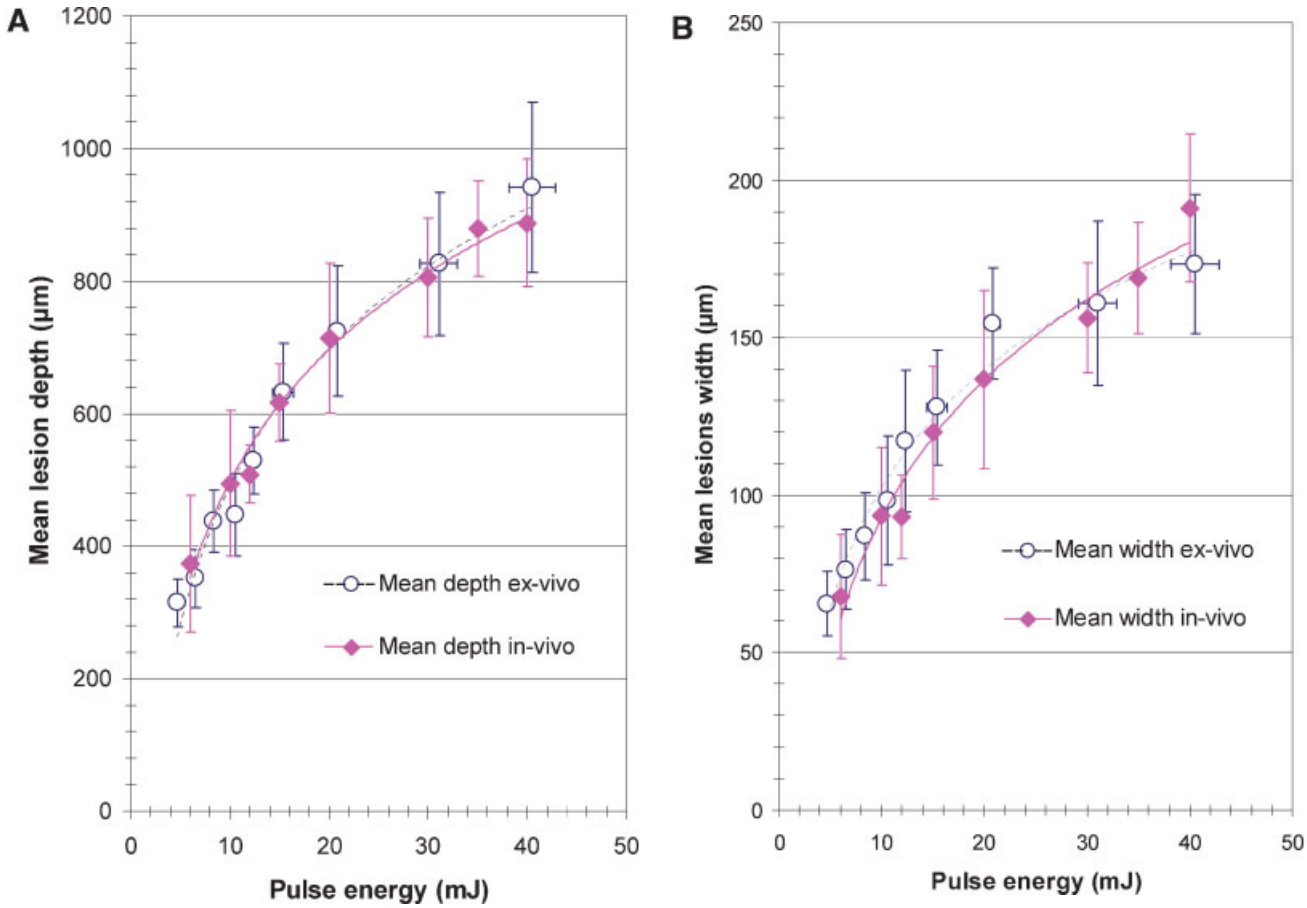

Fig. 5. Plot of mean MTZ depth (**A**) and width (**B**) following Fraxel® SR laser treatment of human skin in vivo and ex vivo at varying pulse energies. Results depict measurements obtained from H&E stained sections. Plot (B) is used to generate the dosimetry chart on Figure 7.

lesion depths and eight for lesion widths, from pulse energies 6 through 40 mJ), validating our ex vivo model as an acceptable methodology for fractional lesion evaluation. The depth-to-width ratios of the ex vivo lesions at all energy parameters remained relatively constant with a mean of 5.2 ± 0.6 based on H&E stain histology.

DISCUSSION

In this report, we have described the physical shapes and sizes of MTZs created during nonablative fractional resurfacing with the Fraxel® SR laser system. An ex vivo model was presented that showed strong statistical agreement in the characteristic lesion shape and size to in vivo histological samples. Obviously, the ex vivo model does not exactly replicate in vivo skin. For example, even with the use of a hot plate, the epidermal-dermal thermal gradient may differ ex vivo versus in vivo. In addition, in the absence of perfusion, excess local heat may dissipate more slowly. Finally, tissue hydration status likely differs between the two systems. We attempted to overcome these limitations by utilizing a hot plate to warm the ex vivo tissue and saline-soaked gauze to hydrate it. Our results indicate that these maneuvers were adequate since the measured in vivo mean lesion depths and widths were not found to be statistically different than the ex vivo measurements with the exception of 3 data points out of 16. It is observed from Figure 5A,B that the mean values of the lesion depths and widths increased as a function of increasing pulse energy. In both the in vivo and ex vivo models, our results showed no statistical difference among the lesion dimensions of pulse energy levels with an increment of less than 5 mJ. This did not mean there was no actual difference between a 6 and 10 mJ treatment, for example, but rather because of a small change in pulse energy, tissue inhomogeneity within the same specimen, and systematic errors during histological processing and lesion analysis did not yield results that allow us to observe any statistical differences in lesion dimensions. Beyond an increment of 5 mJ or more (i.e., say 10 vs. 15 mJ, etc.), the lesion dimensions were indeed found to be statistically different ($P < 0.05$).

Tissue processing techniques also played an important role in the histologic and statistical evaluations. Paraffin and frozen embedding and sectioning techniques were both

found to be useful. Formalin fixing and paraffin embedding enhanced the skin's resistance to stretching and tearing during slicing compared to tissue embedded in OCT compound. For this reason, we support the use of paraffin sections when preservation of innate morphology is important. For example, in each of the frozen sections (Fig. 1B, e.g.), a large separation was observed between the DE junction. These separations are also seen in paraffin sections (Figs. 1A and 4E–H, e.g.), but the separations are typically smaller than the corresponding frozen sections. In both types of processing, these separations are likely the result of laser-induced weakening of the DE junction and processing artifacts. The laser treatment weakens the DE junction which could be further exaggerated by stretching during slicing.

Frozen sections are considerably quicker and simpler to process and the MTZ lesion dimensions for frozen sections were not statistically different from those obtained from the paraffin sections (data not shown). For this reason, frozen sections are also a good choice for identifying trends in lesion dimensions where a large number of samples must be processed to obtain statistically relevant data.

One important limitation of the paraffin processing is the requirement for high temperatures during the embedding stage leading to alterations in proteins of interest. For example, in this report, we used H&E and NBTC; the latter of which is sensitive to excessive temperature. NBTC preferentially stains LDH enzyme within viable mitochondrial cells. The paraffin embedding process heats the tissue high enough to disrupt mitochondrial enzyme activity leading to the falsely negative staining by NBTC. Thus, the NBTC stain is not compatible with the traditional paraffin embedding process. For that reason, all of the NBTC stains presented in this report are processed by frozen sectioning.

The results of these two stains appeared qualitatively different for the MTZs created by the Fraxel® SR laser without further statistical analysis. This difference may not be noticeable in other laser treatments where large beam sizes and full thickness thermal damage occurred. However, due to the small beam size and high irradiance of the Fraxel® SR laser, the thermal profile is very sharp and the size of the lesions as measured by H&E or cross-polarization microscopy (to observe variations in collagen birefringence) can be distinctly different from the lesion sizes as measured using the NBTC stain (to observe non-viable zones). This difference may be due to the different temperatures at which collagen denatures and mitochondrial cells necrose. For example, the lesion widths as quantified by NBTC stain appeared larger than those measured with H&E stain (Figs. 5B and 6). The difference appeared reasonable since cell activities are in general more sensitive to temperature rise than collagen is. However, in order to perform a fair statistical analysis of this difference, staining of H&E and NBTC on paired lesions was required. These measurements were beyond the scope of this report and are part of our future study.

Figures 7 and 8 provide an estimate of treatment dosimetry for the Fraxel® SR laser with the percentage

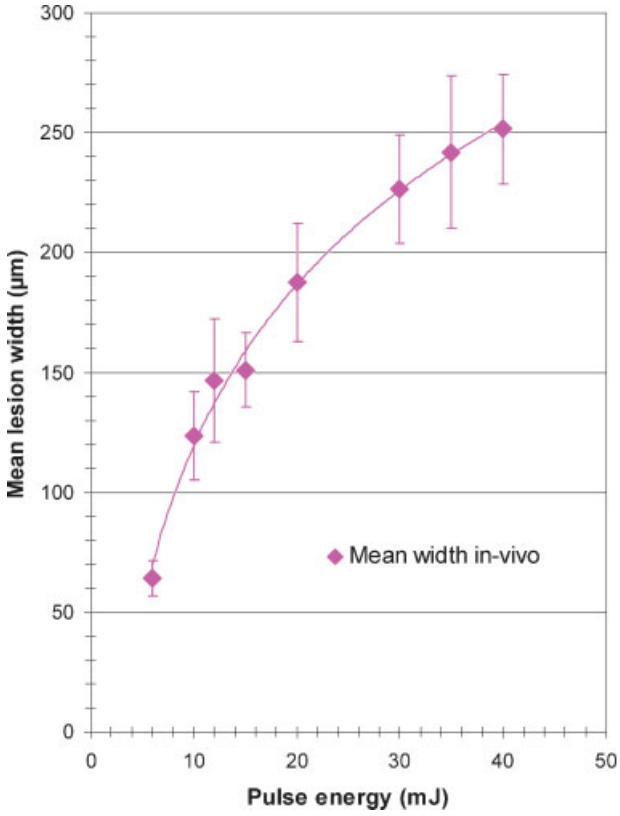

Fig. 6. Plot of mean MTZ width immediately after Fraxel® SR laser treatment of human skin at varying pulse energies. Results depict measurements obtained from NBTC stained sections and are used to generate the dosimetry chart on Figure 8.

of surface treatment coverage as a function of pulse energy. The data shown in Figures 7 and 8 are based on our experimental data presented in Figures 5B and 6, respectively. Note that the percentage treatment coverage or the change in percentage treatment coverage thereof for each set of treatment parameter (i.e., pulse energy and spot density) is very different in Figures 7 and 8 because the lesion cross-section of MTZs based on H&E (Fig. 5B) and NBTC (Fig. 6) stains are different as discussed in the prior paragraph.

Unlike a previous dosimetry based on H&E stain estimated with a simple additive (superposition) method of individual MTZ for multi-pass treatments, the probability of lesion or MTZ overlay due to multi-pass treatments at a spot density setting of 250 MTZ/cm^2 was accounted for in these derivations in Figures 7 and 8. These dosimetry analyses do assume that no bulk heating of clinical consequence resulted from the multi-pass treatments. In general, the key to avoiding clinical bulk heating was to ensure the time internal between every two successive passes are adequately long (i.e., >20 seconds) for the heat to be carried away through thermal diffusion and blood perfusion. Support for this assumption came from histological sections of specimens performed at higher

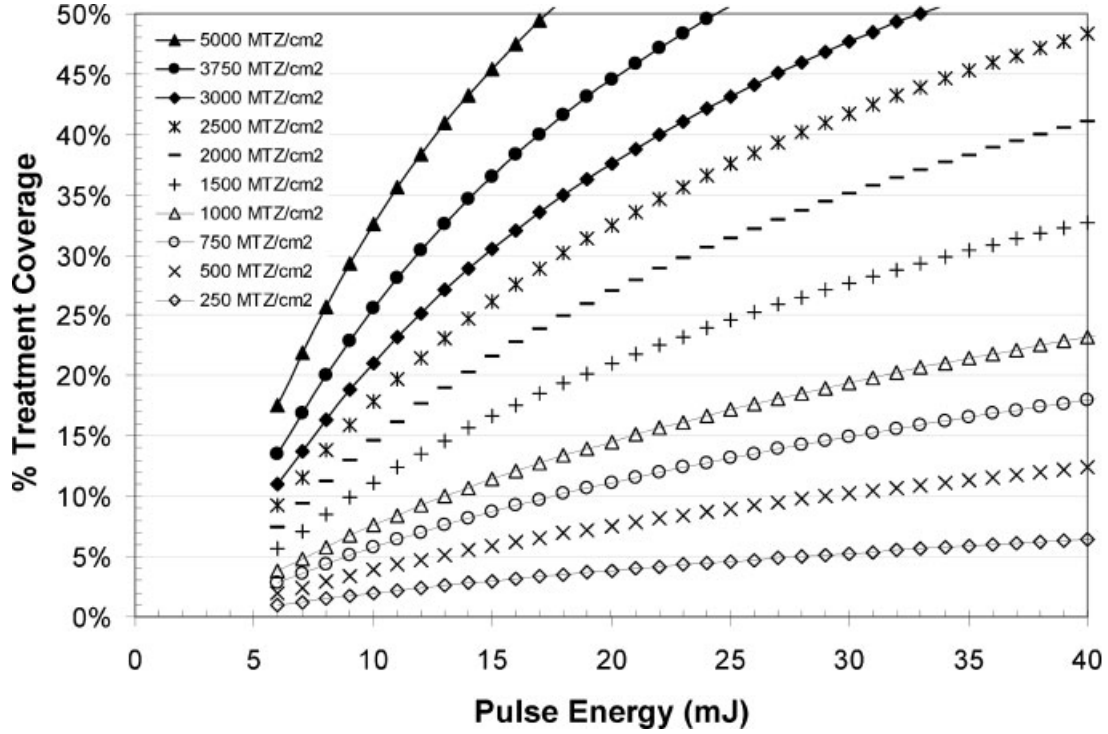

Fig. 7. Dosimetry calculation based on H&E measurements derived in Figure 5B at a per-pass spot density of 250 MTZ/cm^2. The data accounts for the probability of lesion overlay from subsequent passes.

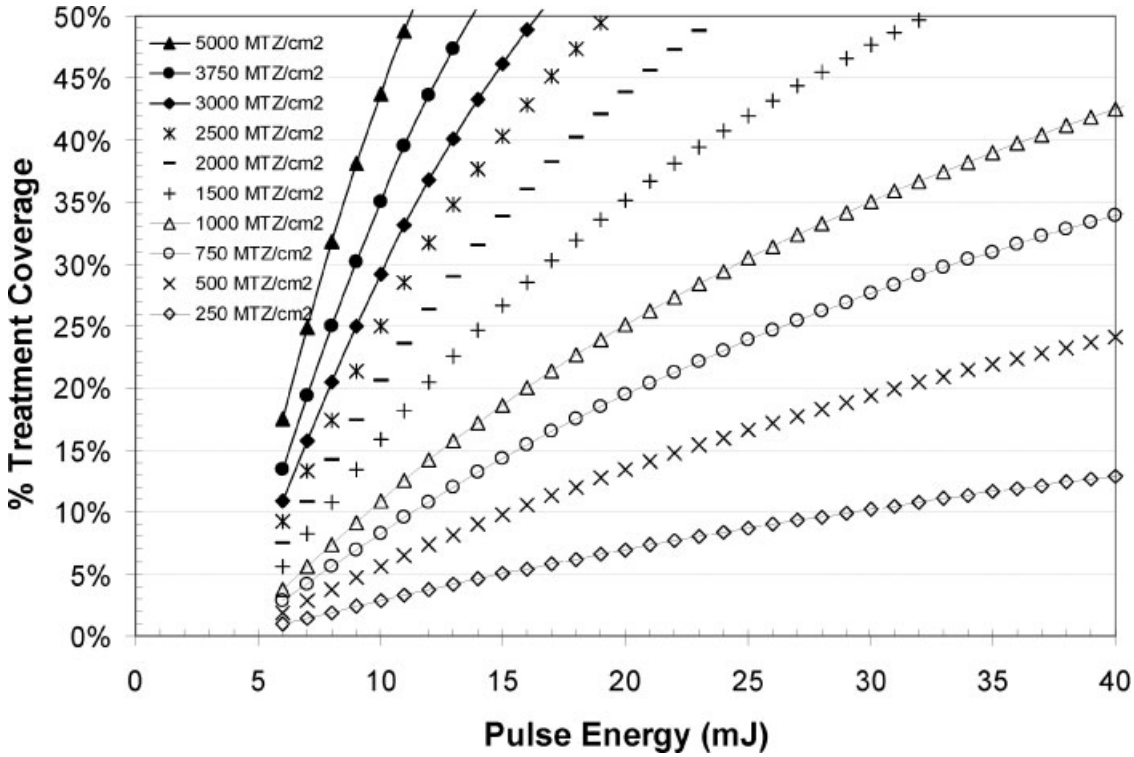

Fig. 8. Dosimetry calculation based on NBTC measurements derived in Figure 6 at a per-pass spot density of 250 MTZ/cm^2. The data account for the probability of lesion overlay from subsequent passes.

per-pass and total percentage coverage showing interlesional tissue sparing but are not presented here as they are beyond the scope of this article. However, treatments beyond 20 mJ at a single-pass spot density setting of 250 MTZ/cm^2 are not recommended. A 125 MTZ/cm^2 setting is available for treatments at higher pulse energies.

In Figure 7, at 20 mJ for a total of 1,000 MTZ/cm^2 based on a 250 MTZ/cm^2 per-pass treatment, the treatment coverage calculation yielded an approximately 15% of cross-sectional collagen denaturation or coagulation zones based on H&E stain as the indicator. This is equivalent to an approximately 25% of cross-sectional necrotic zones with the same parameter set, as shown in Fig. 8, with NBTC stain as the marker. In brief, the fractional modality produced wider coverage of cell necrosis than of collagen denaturation at any pulse energy levels, as indicated by experimental results in Figures 5B and 6. This means that a clinician may intend to treat for a 15% cross-sectional coverage of collagen denaturation or coagulation as an endpoint to promote dermal remodeling, but should be aware that the corresponding percentage coverage of nonviable zone is larger.

The wound healing response to thermal injury requires viable tissue and is thus facilitated by spared interlesional zones. Previous studies have shown non-ablative laser treatment affected zones that extended beyond the immediate area of collagen denaturation and cell death. Capon and Mordon [16] have alluded to the role of heat shock proteins (HSP) in wound healing post non-ablative laser treatment. The heat shock response in spared tissue beyond the immediate thermal damage zone is highly sensitive to temperature rise, resulting in over-expression of HSPs such as HSP 70 which facilitates inflammatory response and wound healing. These heat shock zones may represent a much larger volume of affected tissue as a result of nonablative fractional resurfacing. Further investigation into overexpression of HSPs and other tissue responses such as expression of cytokines and growth factors is ongoing and will help shed light on the effect of fractional treatment on wound healing biology. The present report describes dosimetry based on the size of zones of coagulated or non-viable tissue. In future reports, alternate dosimetry will be developed based on the size and intensity of zones of heat shock and inflammatory response. These alternate dosimetry descriptions may be useful for describing the extent or magnitude of the wound healing response to nonablative fractional resurfacing.

The dosimetry charts based on collagen denaturation and cell death zones are conservative estimates of the extent of fractional treatment. However, they are important as they serve as a reliable reference for the physicians to select the desired surface treatment coverage or the intensity of a treatment. On the other hand, the desired treatment depths can be chosen based on Figure 5A (a plot of lesion depth vs. pulse energy), independent of the cross-sectional treatment coverage. For instance, treatments of epidermal lesions (e.g., lentigines) or the papillary dermis (e.g., dermal melasma) may require lower energies (Fig. 4A–C), compared to deep dermal or scar tissue (e.g., acne scarring or striae) which may require the opposite treatment settings (Fig. 4D–H). Having the freedom to independently choose depth and coverage allows the physician to tailor the treatment to a desired clinical indication.

CONCLUSION

The Fraxel® SR laser system creates an array of microscopic wounds that stimulate collagen remodeling and epidermal turnover. This report describes the trends in treatment coverage area and lesion depth as pulse energy is changed. This information will allow physicians to independently choose coverage area and treatment depth for a given treatment. For substantially deeper treatments, density must be reduced accordingly to avoid adverse effects such as blistering. This report describes how the physical dimensions of microscopic treatment zones (MTZs) created during fractional treatment vary with pulse energy. These measurements are translated into a dosimetric representation to provide treating physicians guidelines when employing a variety of treatment parameters. An ex vivo model has also been developed and validated to allow more rapid exploration of the physical lesion dimensions.

ACKNOWLEDGMENTS

We thank Brad Hauser, Kerrie Jiang, and Heather Tanner for their assistance in carrying out the experiments described in this report. We thank Len DeBenedictis and Rox Anderson, MD, for their guidance and for sharing their considerable insights.

REFERENCES

1. Manstein D, Herron S, Sink K, Tanner H, Anderson R. Fractional photothermolysis: A new concept for cutaneous remodeling using microscopic patterns of thermal injury. Lasers Surg Med 2004;34:426–438.
2. Hruza GJ. Laser skin resurfacing. Arch Dermatol 1996;132: 451–455.
3. Waldorf HA, Kauvar ANB, Geronemus RG. Skin resurfacing of fine to deep rhytides using a char-free carbon dioxide laser in 47 patients. Dermatol Surg 1995;21:940–946.
4. Lowe NJ, Lask G, Griffin ME. Laser skin resurfacing: Pre- and post-treatment guidelines. Dermatol Surg 1995;21: 1017–1019.
5. Lowe NJ, Lask G, Griffin ME, Maxwell A, Lowe P, Quilada F. Skin resurfacing with the Ultrapulse carbon dioxide laser: Observations on 100 patients. Dermatol Surg 1995;21:1025–1029.
6. Lask G, Keller G, Lowe N, Gormley D. Laser skin resurfacing with the SilkTouch flashscanner for facial rhytides. Dermatol Surg 1995;21:1021–1024.
7. David LM, Sarne AJ, Unger WP. Rapid laser scanning for facial resurfacing. Dermatol Surg 1995;21:1031–1033.
8. Ho C, Nguyen Q, Lowe NJ, Griffin ME, Lask G. Laser resurfacing in pigmented skin. Dermatol Surg 1995;21:1035–1037.
9. Fitzpatrick RE, Goldman MP, Satur NM, Tope WD. Pulsed carbon dioxide laser resurfacing of photoaged facial skin. Arch Dermatol 1996;132:395–402.
10. Zachary CB. Modulating the Er:YAG laser. Lasers Surg Med 2000;26:223–226.
11. Khatri KA, Ross V, Grevelink JM, Magro CM, Anderson RR. Comparison of erbium:YAG and carbon dioxide lasers in resurfacing of facial rhytides. Arch Dermatol 1999;135(4): 391–397.

12. Tunnell JW, Chang DW, Johnston C, Torres JH, Patrick CW, Jr., Miller MJ, Thomsen SL, Anvari B. Effects of cryogen spray cooling and high radiant exposures on selective vascular injury during laser irradiation of human skin. Arch Dermatol 2003;139(6):787–788.
13. Khan MH, Bedi VP, Chan KF, Sink RK, Nelson JS. Topically applied optical clearing agent increases the depth of microscopic treatment zones. Lasers Surg Med 2005; Supp 17:31.
14. Chung JH, Koh WS, Youn JI. Histological responses of port wine stains in brown skin after 578nm copper vapor laser treatment. Lasers Surg Med 1996;18(4):358–366.
15. Pierce MC, Sheridan RL, Hyle Park B, Cense B, de Boer JF. Collagen denaturation can be quantified in burned human skin using polarization-sensitive optical coherence tomography. Burns 2004;30(6):511–517.
16. Capon A, Mordon S. Can thermal lasers promote skin wound healing? Am J Clin Dermatol 2003;4(1):1–12.